A novel monochromator with offset cylindrical lenses and its application to a low-voltage scanning electron microscope

Authors

Takashi Ogawa,[1,2,*] Yu Yamazawa,[3] Satoshi Kawai,[3] Atsushi Mouri,[3] Junichi Katane,[3] In-Yong Park,[1,2] Yoshizo Takai,[4] and Toshihide Agemura[3]

Affiliations

[1]Advanced Instrumentation Institute, Korea Research Institute of Standards and Science, 267 Gajeong-ro, Yuseong, Daejeon 34113, Republic of Korea

[2]Major in Nano Science, University of Science and Technology, 217 Gajeong-ro, Yuseong, Daejeon 34113, Republic of Korea

[3]Hitachi High-Tech Corporation, 882 Ichige, Hitachinaka, Ibaraki 312-8504, Japan

[4]Department of Material and Life Science, Graduate School of Engineering, Osaka University, 2-1 Yamada-oka, Suita, Osaka, Japan

*Corresponding author

Tel: +82-42-868-5920, Fax: +82-42-868-5827,

E-mail address: togawa@kriss.re.kr (T. Ogawa).

Supplementary Materials

S1. SEM Resolution by the Derivative (DR) Method

The SEM resolving performance is evaluated with the derivative (DR) method. The details are described in an ISO technical specification (ISO/TS24597, 2011). An edge resolution, or an image sharpness as an exact expression in the ISO document, is evaluated for an SEM image in the following manners.

Considering that a beam profile is a Gaussian distribution with a standard deviation σ and a specimen edge is given as an ideal step function, a line profile at the edge is given as

$$y = \frac{1}{2}\left(1 + \mathrm{erf}(x/\sqrt{2}\,\sigma\right), \tag{S1}$$

where the error function erf is defined as $\mathrm{erf}(x) = \frac{2}{\sqrt{\pi}}\int_0^x e^{-t^2}\,dt$. Then, the edge resolution, that is, a rising distance between signal levels of 25 and 75% of the line profile corresponds to$\sqrt{2}\sigma$.

The software automatically detects a large number of edges of particles in an SEM image and derives multiple line profiles. The number of measurement positions is usually over 1000. The software applies an error function fitting for a measured line profile with an equation of

$$y = b + h * \left[0.5 + 0.5\,\mathrm{erf}\left((x - m)/\sigma\sqrt{2}\right)\right]. \tag{S2}$$

After filtering out results with insufficient values, the values of σ, which are derived from multiple line profiles, are averaged. The parameter $\sqrt{2}\sigma$ corresponds to the edge resolution of the SEM image.

S2. Measurement of SEM Resolutions

In this article, the SEM resolving performance is evaluated with the derivative (DR) method. Supplementary results of the measurement of the SEM resolution are shown in this section. In Figs. S1, a large number of light blue lines at the edges of the particles show the locations of the measured line profiles. The measured resolutions of the line profiles are summarized as a histogram in Fig. 6c. Figs. S1 also shows white circles with radial lines at the center, which visualize the measured resolution in each direction. The comparison of the sizes of the two white circles in Figs. S1a and b implies that the MC improved the SEM resolution. For other SEM images in Figs. 6 and 7, the resolutions were measured similarly.

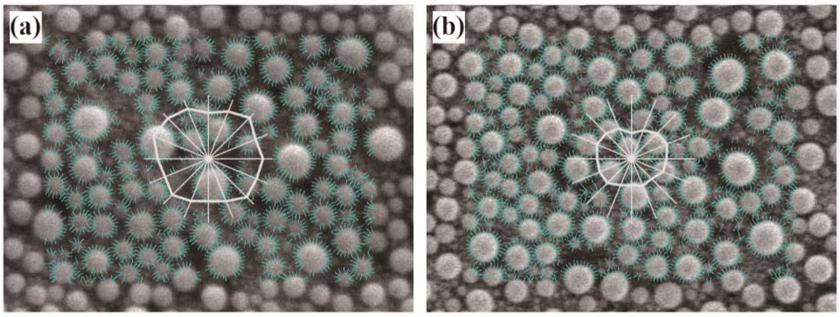

Fig. S1 Screen-captured images of the resolution evaluation software for SEM images (a) without and (b) with the MC.

S3. Comparison of SEM Images under Equivalent Dose Conditions at 0.5 keV

In this section, supplementary results on the SEM images are shown for comparing the image quality in equivalent dose conditions when the MC turned on or off. Figures S2 shows SEM images of a Cu mesh (a) without and (b) with the MC at 0.5 keV. The frame doses per image were 67 pC and the same for two images. Fig. S2b is identical to Fig. 5b. Except for the dose, other observation conditions in Fig. S2a were the same as those in Fig. 5a. As a result of the visual evaluation, the SEM image with the MC in Fig. S2b is significantly better than that without the MC in Fig. S2a. When comparing SEM images without the MC, Fig. S2a is worse than Fig. 5a because Fig. S2a was acquired in the lower dose condition. This dependence of the image quality on the dose is discussed in the main manuscript based on the references by Sato (2016).

Figures S3 show SEM images of Sn particles (a) without and (b) with the MC at 0.5 keV. Additionally, the SEM image in Fig. S3c was acquired with an original FE-SEM (SU5000) equipped with a conventional Schottky emitter (SE) gun. A probe current was 7.5 pA in Fig. S3c, which was the lowest current among standard operation conditions available for users. Fig. S3b is identical to Fig. 6e. The frame doses were almost equivalent among the three SEM images in Fig. S3. After visually evaluation, the SEM image with the MC in Fig. S3b is better than the other two SEM images in Figs. S3a and c. For two SEM images without the MC, even though the probe current in Fig. S3c was reduced approximately by one-fourth to that in Fig. S3a, this reduction gives no improvement of the SEM image quality. This is also supported by the theoretical study on the SEM resolution without the MC for different probe currents. It is also noted that both Figs. S3a and S3c are worse than Fig. 6d because of the lower dose conditions.

As a result of comparing the SEM images under equivalent doses or reduced current conditions, the SEM images with the MC are of the best quality. These supplemental results support the results and discussion in the main manuscript.

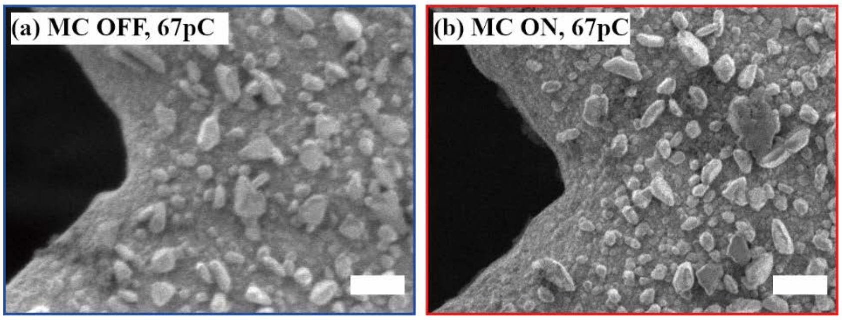

Fig. S2. SEM images (a) without and (b) with the MC at 0.5 keV at equivalent dose conditions. Fig. S2b is identical to Fig. 5b. The specimen was a Cu mesh and the scale bar is 1 μm. The probe currents were (a) 36 pA without the MC and (b) 1.4 pA with the MC. The frame doses are shown in figure labels.

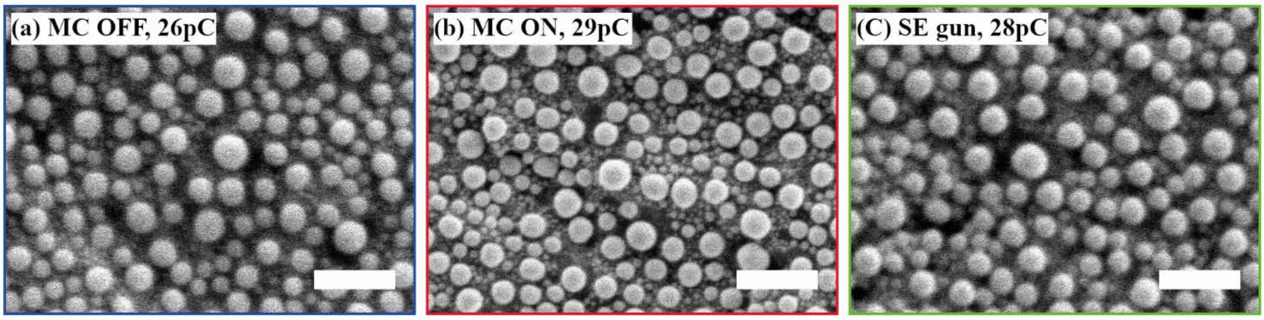

Fig. S3. SEM images (a) without and (b) with the MC at 0.5 keV at equivalent dose conditions. The SEM image (c) was acquired with a conventional Schottky emitter (SE) gun. The scale bar is 500 nm. The frame doses are shown in figure labels. The probe currents were (a) 28 pA without the MC, (b) 0.6 pA with the MC, and (c) 7.5 pA with the SE gun.

S4. An Artifact of Energy Spectrum with a Retarding Field Energy Analyzer

In this section, a supplementary explanation is given on an artifact of the energy spectrum with the MC in Fig. 4. Especially, the cause of the irregular shoulder in the low-energy tail is discussed in detail. The energy spectra in Fig. 4 were acquired with a retarding field energy analyzer (RFA), which is shown as a schematic on the left side of Fig. 1. The RFA has an advantage in the compatibility of two functions: observing beam profiles by a phosphor screen and measuring energy spreads. This is beneficial for the evaluation of the MC optics in the initial step. Figure S4 shows the dependence of the RFA signal on the energy when the MC was turned on. Fig. S4 was obtained by measuring the screen signal by changing a voltage to the RFA by 5 mV step. The negative conversion of the RFA voltage corresponds to the electron energy. The RFA voltage sets the threshold energy, which means that electrons with higher energy can overcome the threshold and reach the detector, but the other electros with lower energy can not overcome the threshold and be repelled backward without the detection. Therefore, the RFA is considered to be a high-pass energy filter, which requires differentiation of the signals for acquiring actual energy spectra. By numerically differentiating the signal in Fig. S4 after applying the smoothing process, the energy spectrum with the MC was obtained in Fig. 4.

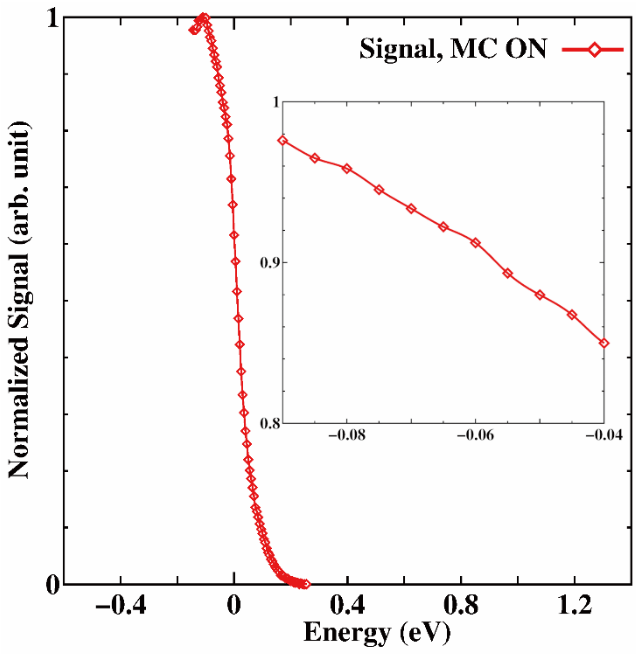

Fig. S4. Dependence of the RFA signal on the energy when the MC was turned on. The differentiation of the RFA signal corresponds to the energy spectrum with the MC in Fig. 4. The horizontal scale is the same in Fig. S4 and Fig. 4. Inset is the enlarged graph of the RFA signal, which shows the corresponding region of the shoulder in the tail of the energy spectrum in Fig. 4.

The inset of Fig. S4 shows the enlarged graph in the region corresponding to the shoulder in the low-energy tail of the energy spectrum in Fig. 4. In the inset of Fig. S4, the signal decreases monotonically as the energy increases. When observed in detail, the signal fluctuates from the decreasing trend, which means that a difference, or an incline, of the plot changes at each step. This amplitude of the signal fluctuation is very small. However, the application of the differentiation process to the fluctuation magnifies the amplitude distinctly and generates the shoulder in the tail of the energy spectrum in Fig. 4. The main reason for this small fluctuation is considered to be the aberration of the RFA, which means that the

RFA inhomogeneously influences the beam trajectories for the beam with different initial conditions such as the incident positions, angles, and energies. The requirement of the differentiation process for acquiring spectra is an intrinsic and inevitable shortcoming of the RFA, which causes several types of artifacts: sub-peaks around the zero level, split peaks, asymmetry, and long tails. The irregular shoulder in Fig. 4 is also one of the typical symptoms. Similarly, this shoulder was also found in the energy spectra measured with the RFA in the references by Cui et al. (2004) and Muro et al. (2017).

Even though the energy spectrum in Fig. 4 has the shoulder in the tail, this does not cause any influence on the discussion of this study. The energy spectra in Fig. 4 were principally used for estimating the energy spreads (δE) in FWHM (the width of 50% of the peak) when the MC was turned on and off. Then, the energy spreads were applied for calculating the chromatic aberration of Eq. 1, and the theoretical spatial resolutions of the SEM were determined in low-energy conditions. Because the shoulder in Fig. 4 is located at approximately 30 % of the maximum value, this does not give any influence on the measured FWHM energy spread. Furthermore, the energy spectra in Fig. 4 and the energy spreads in Table 1 clearly show the energy-reducing effect of the MC by comparing two conditions with the MC turned on or off.

As a conclusion of this section, the irregular shoulder of the energy spectrum is attributed to the differential process, which magnifies the signal fluctuation with the small amplitude in the RFA signal to the noticeable level in the energy spectrum. This is one of the typical artifacts of the retarding field energy analyzer. Despite the shoulder, the energy spectra in Fig. 4 are sufficient to support the discussion in this study.

Reference

Cui, Y., Zou, Y., Valfells, A., Reiser, M., Walter, M., Haber, I., Kishek, R. A., Bernal, S., O'Shea, P. G. (2004). Design and operation of a retarding field energy analyzer with variable focusing for space-charge-dominated electron beams. *Review of Scientific Instruments* **75**, 2736. https://doi.org/10.1063/1.1777384.

ISO/TS24597 (2011). Microbeam analysis - Scanning electron microscopy - Methods of evaluating image sharpness.

MURO, T., OHKOCHI, T., KATO, Y., IZUMI, Y., FUKAMI, S., FUJIWARA, H., MATSUSHITA, T. (2017). Wide-angle display-type retarding field analyzer with high energy and angular resolutions. *Review of scientific instruments* **88**, 123106. https://doi.org/10.1063/1.4990769.

SATO, M. (2016). Electron Optics for Scanning Electron Microscope (SEM). *KENBIKYO* **51**, 37–42. http://microscopy.or.jp/archive/magazine/51_1/51_1e09ms.html.